Simulation study of a high-performance brain PET system with dodecahedral geometry

Weijie Tao
School of Biomedical Engineering, Shanghai Jiao Tong University, Shanghai 200240, China
Department of Nuclear Medicine, Ruijin Hospital, Shanghai 200240, China

Gaoyu Chen and Fenghua Weng
School of Biomedical Engineering, Shanghai Jiao Tong University, Shanghai 200240, China

Yunlong Zan
University of Michigan - Shanghai Jiao Tong University Joint Institute, Shanghai Jiao Tong University, Shanghai 200240, China

Zhixiang Zhao
School of Biomedical Engineering, Shanghai Jiao Tong University, Shanghai 200240, China

Qiyu Peng[a)]
Lawrence Berkeley National Laboratory, Berkeley, 94720 CA, USA

Jianfeng Xu[a)]
School of Mechanical Science and Engineering, Huazhong University of Science and Technology, Wuhan, Hubei 430074, China

Qiu Huang[a)]
School of Biomedical Engineering, Shanghai Jiao Tong University, Shanghai 200240, China
Department of Nuclear Medicine, Ruijin Hospital, Shanghai 200240, China

(Received 27 November 2017; revised 16 May 2018; accepted for publication 16 May 2018; published 14 June 2018)

Purpose: In brain imaging, the spherical PET system achieves the highest sensitivity when the solid angle is concerned. However, it is not practical. In this work, we designed an alternative sphere-like scanner, the dodecahedral scanner, which has a high sensitivity in imaging and a high feasibility to manufacture. We simulated this system and compared the performance with a few other dedicated brain PET systems.
Methods: Monte Carlo simulations were conducted to generate data of the dedicated brain PET system with the dodecahedral geometry (11 regular pentagon detectors). The data were then reconstructed using the in-house developed software with the fully three-dimensional maximum-likelihood expectation maximization (3D-MLEM) algorithm.
Results: Results show that the proposed system has a high-sensitivity distribution for the whole field of view (FOV). With a depth-of-interaction (DOI) resolution around 6.67 mm, the proposed system achieves the spatial resolution of 1.98 mm. Our simulation study also shows that the proposed system improves the image contrast and reduces noise compared with a few other dedicated brain PET systems. Finally, simulations with the Hoffman phantom show the potential application of the proposed system in clinical applications.
Conclusions: In conclusion, the proposed dodecahedral PET system is potential for widespread applications in high-sensitivity, high-resolution PET imaging, to lower the injected dose. [https://doi.org/10.1002/mp.12996]

Key words: dodecahedral PET system, Monte Carlo simulation, system evaluation

1. INTRODUCTION

The application of dedicated brain Positron Emission Tomography (PET) system in brain imaging[1] dates back to almost two decades ago. Although different designs of PET systems such as hexagonal[2] and spherical[3] geometries have been proposed, the most popular clinical PET system is composed of detector modules of stacking rings.[4] The ring detector PET might be a good choice for whole body imaging while not optimized for specific organs such as the brain, due to the low sensitivity. In order to increase image quality of the PET brain imaging, dedicated brain PET systems were designed with small diameter detector rings, such as the High-Resolution Research Tomograph (HRRT) system[5,6] and the one with four-layer MPPC DOI detectors.[7,8] However, the sensitivity of these ring detector systems degrades heavily with the increase of the distance from axis in the transaxial plane.[9] The low sensitivity of the peripheral area in FOV affects quantitative accuracy for some brain regions, such as parts of cerebellum region,[10] while the cerebellum region is vital for brain imaging because this region is usually used as the reference area.[11] In addition, the low sensitivity of these ring PET systems hampers the development of low-dose PET imaging.[12]

Recently several designs of dedicated brain systems have been presented. Gong et al.[13] simulated a helmet structure system that consists of six side rings with different diameters, a top panel, and a bottom panel. A slightly different helmet PET was first presented and then upgraded to the helmet-chin system.[14–17] The scanner enhances the imaging performance for both bottom and top region of the brain. Moghaddam et al.[18] designed a spherical brain PET system with liquid xenon detectors, with a large solid angle[19] but much complexity in realization in practice. Our previous study[20] has assessed different geometric brain PET systems with large solid angels and found that the dodecahedral PET was a reasonable approximation of the spherical cap PET.

In this study, we simulated this dedicated brain PET system with the dodecahedral geometry using the GATE toolkit.[21] The system performance has been evaluated in term of sensitivity, spatial resolution, count rate, and reconstructed image quality, compared to the helmet system designed by Gong et al.,[13] the helmet-chin PET proposed by Ahmed et al.,[17] and the HRRT brain PET system.[5]

2. MATERIALS AND METHODS

2.A. System design

The dedicated dodecahedral brain PET scanner consists of 11 flat depth-of-interaction (DOI) detector modules and an open face, as shown in Fig. 1. All detector modules and the open face are pentagons of the same size. The inscribed circle of the pentagon has a radius being 9.28 cm. The dodecahedron has an inscribed sphere with radius 15 cm. In other words, the distance from the center to each detector plane is 15 cm, which makes every two opposite modules 30 cm apart. The circumradius of dodecahedron is 18.8 cm so that the longest distance between two points in the scanner does not exceed 37.6 cm. The detectors consist of high-density pixelated-LYSO crystals with the size of 2 × 2 × 20 mm (thickness). All simulation parameters are summarized in Table I.

We constructed the structure of dodecahedron in GATE v7.1 with the "generic repeater" function and analyzed the simulated data in the ROOT program package.[22] In all simulations of the dodecahedral scanner, unless otherwise specified, the energy window was chosen to be 250–750 keV with the energy resolution being 14%, and the coincidence timing window was 6 ns. Parallax errors affect spatial resolution[23] even at the center of the proposed system since gamma rays emitted from the center may enter crystals obliquely. We added the DOI information to reduce the parallax error.[24]

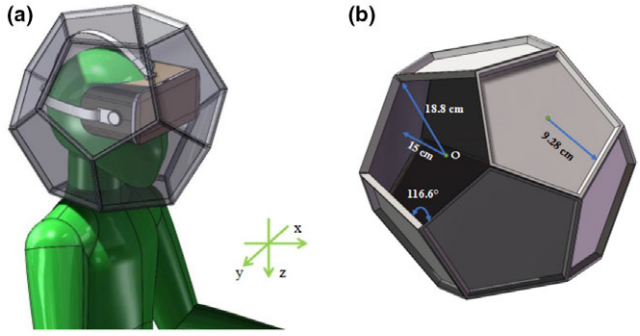

FIG. 1. Geometry of the proposed dodecahedral scanner. (a) Conceptual illustrations of the proposed scanner. (b) Geometrical dimension of the scanner. [Color figure can be viewed at wileyonlinelibrary.com

TABLE I. Simulation parameters of the proposed brain PET.

	Parameters
Crystal material	LYSO
Crystal size (mm^3)	2 × 2 × 20
Inradius (cm)	15
Circumradius (cm)	18.8
Angle between adjacent faces (degree)	116.6
Open face inscribed circle radius (cm)	9.28
Energy window (keV)	250–750
Energy resolution	14%
Coincidence timing window (ns)	6

2.B. Phantoms

To evaluate the performance of our proposed brain system, we simulated six phantoms to be consistent with those for the helmet system,[13] the helmet-chin PET,[17] and the HRRT system.[5] Table II lists all six phantoms. The first three of them were directly defined in GATE. The uniform water cylinder phantom, with a diameter of 24.5 cm and the axial length of 19 cm,[13] was used for comparison of sensitivity. And a hemisphere phantom with a diameter of 22.8 cm[17] was used to assess the noise equivalent count rate (NECR). Besides, the point source phantom was designed to measure the resolution at different positions in the FOV. It consists of 19 radioactive point sources either placed along the positive X-axis in the plane Z = 0 cm or along the Z-axis. All point sources have a diameter of 1 mm, and are 2 cm apart from the adjacent source. The last three phantoms, Derenzo phantom, Jaszczak phantom,[25] and Hoffman phantom,[26] were imported into GATE.

2.C. Image reconstruction

The simulated PET data were reconstructed using our in-house developed reconstruction software. The software was

TABLE II. Digital phantoms. D stands for diameter. L stands for axis length.

Phantom	Physical dimensions (mm)	Application
Cylinder	D: 245 L: 190[13]	Sensitivity
Hemisphere	D: 228[17]	NECR
Point sources	D: 1	Spatial resolution
Derenzo	D: 2.4, 3.4, 5.0, 6.6, 8.4, 9.8	Spatial resolution
Jaszczak	D: 14.4, 19.2, 27.2, 33.6, 43.2, 59.2	Contrast/Noise
Hoffman	Sagittal: 224, Coronal: 224, Vertical: 180	Image visualization

TABLE III. Sensitivities of different geometries.

System	Sensitivity	Scatter fraction
HRRT PET	1.04%	36.24%
Helmet	3.58%[13]	31.20%[13]
Dodecahedral PET	6.15%	33.90%

developed according to the fully three-dimensional maximum-likelihood expectation maximization (3D-MLEM) algorithm on list mode data.[27] We have validated our software via reconstructions of images for the ECAT[28] and mCT[29] systems using Software for Tomographic Image Reconstruction (STIR)[30] as the benchmark. Throughout this study, 20 iterations were used in the reconstruction. The matrix size of reconstructed images was set to 256 × 256 × 250 with a voxel size of 1 × 1 × 1 mm^3 except for the Hoffman phantom, which has a matrix size of 240 × 240 × 80 with a voxel size of 1 × 1 × 2.5 mm^3.

2.D. Performance assessment

The system performance was evaluated using a few metrics explained in this subsection. In order to compare the proposed system with the commercialized system HRRT, we also simulated HRRT with the exact same physics model and calculated these metrics. However, for the helmet and helmet-chin systems, due to their complicated geometries, we referred to figures of merit in literatures.

2.D.1. Sensitivity

The overall sensitivity performance was evaluated using the uniform water cylinder phantom (as in Table II) injected with 1 MBq ^{18}F-FDG. The phantom was positioned in the center of the FOV with its axis along Z-axis. In GATE simulation, true and scattered events were recorded separately. We then obtained the overall sensitivity as the ratio between the number of detected true events and the total number of annihilations in the phantom.

To illustrate the uniformity of sensitivity, the point source was positioned in each voxel of a water sphere with diameter 26 cm, and then spatial sensitivity maps were obtained by calculating the sensitivity at each voxel for planes at specific Z-axis coordinates.

2.D.2. Resolution

Spatial resolution represents the ability of the system to resolve small objects. Two approaches were used to assess the spatial resolution. One measured the size of the reconstructed image of a point source. After the image of the point source was reconstructed and fit with a Gaussian function, the full width at half maximum (FWHM) of the Gaussian function was calculated as the metric. In this study, we used the point source phantom containing 19 points as described in Section 2.B. The other approach used the visual observation on the image of a modified Derenzo phantom. We simulated an injection of 5.7 MBq ^{18}F-FDG with acquisition time being 10 s for this phantom introduced in Table II.

2.D.3. Noise equivalent count rate (NECR)

The NECR of the scanner provides a global measure of the noise performance of the system, since it is not sensitive to regional variations of the source distribution. As in the helmet-chin PET study,[17] NECR was assessed using the hemispherical phantom and the energy window was set as 400–600 keV. At a fixed activity, NECR was calculated using the formula given by Strother et al.[31]:

$$\mathrm{NECR} = \frac{T^2}{T + S + 2R} \tag{1}$$

where T, S, and R are the true, scatter, and random count rates, respectively.

2.D.4. Contrast-to-noise ratio (CNR) and contrast recovery coefficient (CRC)

Noise property in the reconstructed image is essential to clinical practice. To compare the means of CNR and CRC for different systems using the Jaszczak phantom (as in Table II), we simulated an injection of 7 MBq ^{18}F-FDG with acquisition time being 100 s in GATE. The activity concentrations were 3:1 for the hot spheres and the background. In the reconstructed PET images, two types of regions of interest (ROIs) were drawn. One was placed in the background of the image. And the other was placed inside the hot area, covering the entire area of the hot spot. The activity difference between these two ROIs was then normalized by the standard deviation of the background to represent the noise level in the reconstructed images, a.k.a, the contrast-to-noise ratio. Thus,

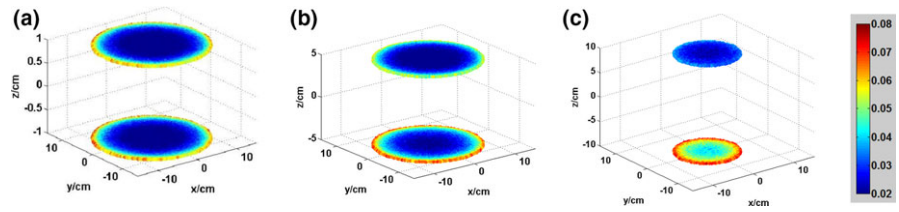

FIG. 2. The distribution of sensitivity in ROI. (a) z = 1 cm and z = −1 cm. (b) z = 5 cm and z = −5 cm. (c) z = 10 cm and z = −10 cm. [Color figure can be viewed at wileyonlinelibrary.com]

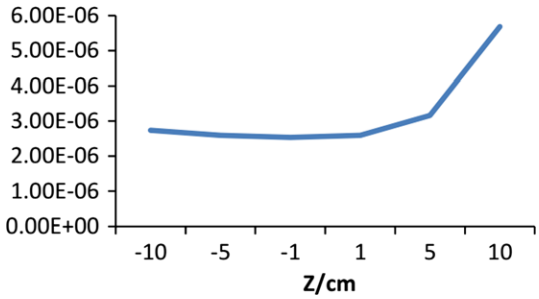

FIG. 3. Standard deviation of sensitivity. [Color figure can be viewed at wile yonlinelibrary.com]

CNR is represented as

$$\mathrm{CNR} = \frac{M_{ROI} - M_{BG}}{NSD} \tag{2}$$

where M_{ROI} and M_{BG} are the evaluated mean activity concentration in the hot ROI and the background ROI, and NSD is the standard deviation of the background ROI.[32]

The CRC is quantified by the percent contrast for each hot ROI as:

$$\mathrm{CRC} = \frac{M_{ROI}/M_{BG} - 1}{\alpha_{ROI}/\alpha_{BG} - 1} \times 100\% \tag{3}$$

where α_{ROI} and α_{BG} are the mean activity concentrations in the hot spheres and background.[5]

3. RESULTS

3.A. Comparison of sensitivity

The overall sensitivity performance is shown in Table III for the proposed system, together with the HRRT system and the helmet PET system.[13] According to the result, our proposed PET system has an improvement in the sensitivity by 72% compared with the helmet system and by 4.91 times compared with the cylinder brain scanner. The scatter fractions of the three systems are also shown in Table III. The result shows that the dodecahedral brain PET has higher scatter fraction respect to the helmet system. This is due to the larger solid angle and smaller solid space of the dodecahedral system.

The spatial sensitivity map is shown in Fig. 2 for six axial planes in the whole FOV of the proposed system. In each transaxial plane, the sensitivity is higher at the edge than in the center section, while higher uniformity is evident in the center region. This is due to the attenuation of the sphere water phantom. As expected, sensitivity decreases along the Z-axis, since the open flat was located at Z = 15 cm. Standard deviation of each slice was calculated to assess the uniformity along the Z-axis. As shown in Fig. 3, higher variation is observed in the transaxial planes closer to the open flat.

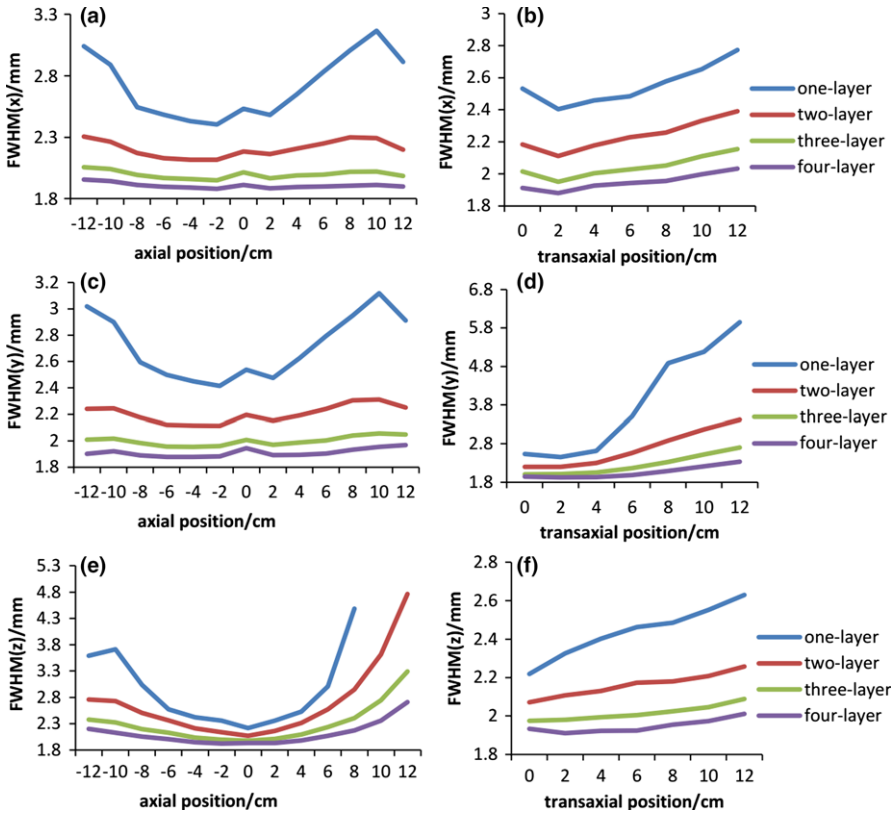

FIG. 4. Effect of DOI on spatial resolution. The first column (a, c, and e) shows FWHM for points along Z-axis, while the second column (b, d, and f) for points along X-axis at Z = 0. From top to bottom, each row shows FWHM along radial, tangential and axial directions, respectively. [Color figure can be viewed at wile yonlinelibrary.com]

3.B. Spatial resolution

To evaluate spatial resolution of the proposed system, we first calculated the FWHM of reconstructed point sources. Due to the high parallax errors of the compact design, the spatial resolution is worse than 2.4 mm. We then included the DOI information to reduce the parallax errors. For DOI detectors, the crystals were divided into multiple layers in the radial direction with equal lengths. We compared FWHM along three directions with DOI resolutions being 20, 10, 6.67, and 5 mm, corresponding to one, two, three, and four layers of crystals. Results are shown separately for points along Z-axis [Figs. 4(a), 4(c) and 4(e)] and along X-axis [Figs. 4(b), 4(d) and 4(f)] in the center plane. It is evident that the more the layers, the better resolution the system achieves. When the DOI resolution is designed to be 6.67 mm, the best spatial resolution of our dedicated brain system is achieved near the center of the FOV, which is 1.98 mm, better than the helmet-chin system (2.5 mm with DOI resolution being 5 mm)[16] and the HRRT system (2.5 mm with DOI resolution being 10 mm).[5] We then chose DOI resolution of 6.67 mm for simulations in the rest of this work.

To assess the spatial resolution via the Derenzo phantom, Fig. 5 shows the center slice of the reconstructed images where each voxel has been normalized to the maximum activity in the image. Our dodecahedral system and the HRRT system are both able to distinguish the smallest rods with the diameter of 2.4 mm, which is better than that of the helmet system (2.7 mm).[13] The profile shows that our system resolves the smallest rods better than the HRRT system.

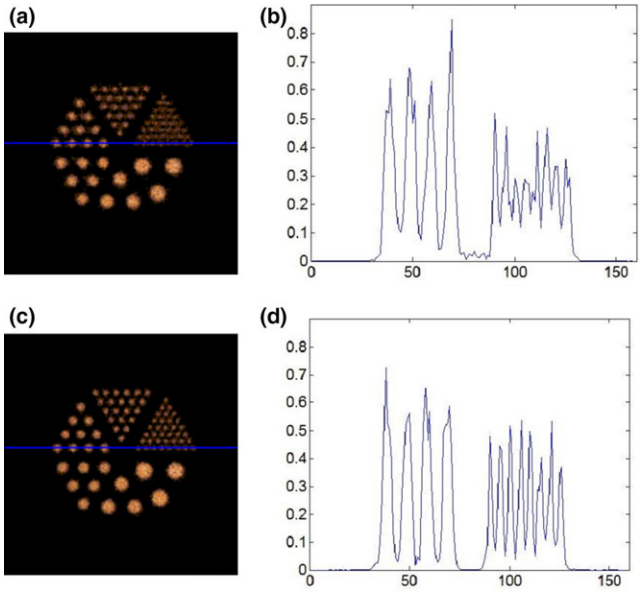

FIG. 5. The reconstructed images for Derenzo phantom from the HRRT system and the dodecahedral system. (a) The center slice for the HRRT system. (b) Profile along the line in (a) corresponding to the hot rods with diameter of 5.0 mm (peaks on the left) and 2.4 mm (peaks on the right). (c) The center slice for the dodecahedral system. (d) Profile along the line in (c) corresponding to the hot rods with diameter of 5.0 mm (peaks on the left) and 2.4 mm (peaks on the right). [Color figure can be viewed at wileyonlinelibrary.com]

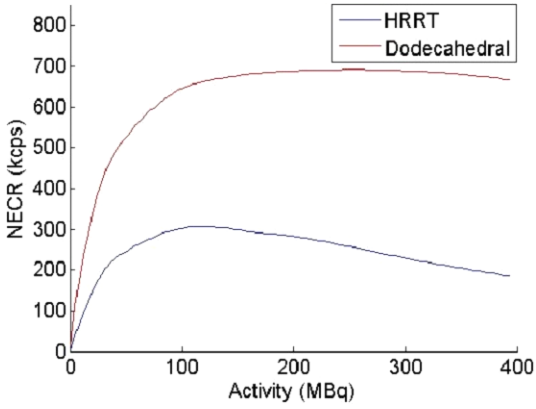

FIG. 6. NECR curves of the HRRT system and the dodecahedral system. [Color figure can be viewed at wileyonlinelibrary.com]

3.C. NECR

The NECR curves of the HRRT system and of our proposed system are reported in Fig. 6. The peak-NECR for HRRT is 307.1 kcps when the phantom is filled with a uniformly distributed activity of 117.5 MBq. The peak-NECR of the dodecahedral system is 691.2 kcps at 258 MBq. The helmet-chin PET has the peak-NECR values of 265 kcps at 55 MBq.[17] Comparison of the peak-NECR is listed in Table IV. Our dodecahedral scanner increases the peak-NECR by 1.61 times compared to the helmet-chin scanner and by 1.25 times compared to the HRRT scanner.

3.D. CNR and CRC evaluations

The CNR values were calculated using Eq. (2) for six hot ROIs indicated by red circles in Fig. 7(a), where the background ROI, as in blue in Fig. 7(a), was chosen to be the disk with 48 mm in diameter at the center of the Jaszczak phan-

TABLE IV. Peak NECR comparison.

Model	HRRT	Helmet-chin	Dodecahedral
NECR(kcps)	307.1	265.0[14]	691.2

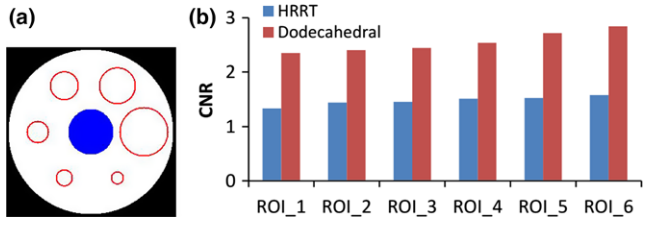

FIG. 7. Comparison of CNR between the dodecahedral system and the HRRT system. (a) ROIs in the hot regions (circles on the edge with diameters of 14.4, 19.2, 27.2, 33.6, 43.2, 59.2 mm) and in the background (circle in the center with diameter of 48 mm). (b) CNR for the six ROIs in the HRRT system and the dodecahedral system. [Color figure can be viewed at wileyonlinelibrary.com]

TABLE V. CRC at contrast level of 3:1.

	14.4 mm	19.2 mm	27.2 mm	33.6 mm	43.2 mm	59.2 mm
HRRT (%)	60.39	65.46	66.04	68.69	69.23	71.69
Dodecahedral (%)	68.95	70.47	71.60	74.39	79.64	83.38

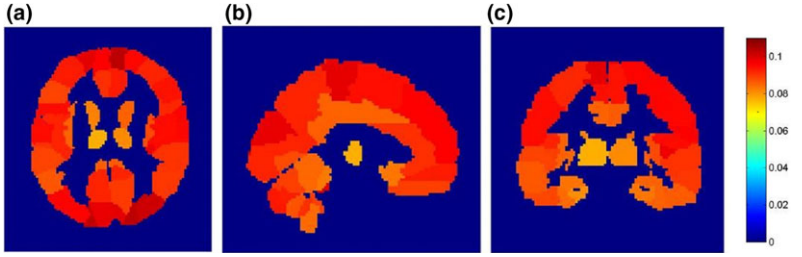

FIG. 8. Three perspectives on the sensitivity of brain regions. (a) Cross section of the brain. (b) Sagittal plane of the brain. (c) Coronal plane of the brain. [Color figure can be viewed at wileyonlinelibrary.com]

tom. Figure 7(b) shows CNRs of the six ROIs for the dodecahedral system and the HRRT system. The proposed dodecahedral system has an average improvement in CNR by 74% compared with the HRRT system.

The percentage CRCs of six ROIs are listed in Table V. The dodecahedral system shows better ability of contrast recovery, compared to HRRT.

3.E. Potential clinical application

To illustrate the potential clinical application of our proposed system, a 3D Hoffman phantom was imported into the GATE toolkit to coordinate the activity distribution with the brain regions. The digital phantom was segmented into 116 volumes of interest (VOIs) based on magnetic resonance images. The average sensitivity of each VOIs of the Hoffman brain phantom was calculated and then the average values were mapped to each corresponding brain regions to obtain the sensitivity map. The sensitivity map of cross section, sagittal plane, and coronal plane were shown in Fig. 8. The average sensitivity around 9% can be observed in brain regions corresponding to a lot of common brain diseases, for instance, the angular gyrus, parietal lobe, occipital lobe, and frontal lobe. The high sensitivity indicates that with the proposed system higher sensitivity (or lower dosage) may be possible in diagnose of some brain diseases such as Alzheimer and Parkinson. Besides, we planned to integrate the system with virtual reality goggles to image patients with claustrophobia and to perform other cognitive studies.

For the Hoffman phantom data, we simulated an injection of 2.67 MBq ^{18}F-FDG with acquisition time being 1000 s. Figure 9 compares three representative (top, middle, and bottom) slices of the Hoffman phantom reconstructions for the dodecahedral PET system and the HRRT system. For all slices, the dodecahedral PET produces images with lower noise than the HRRT system. This is consistent with the sensitivity improvement.

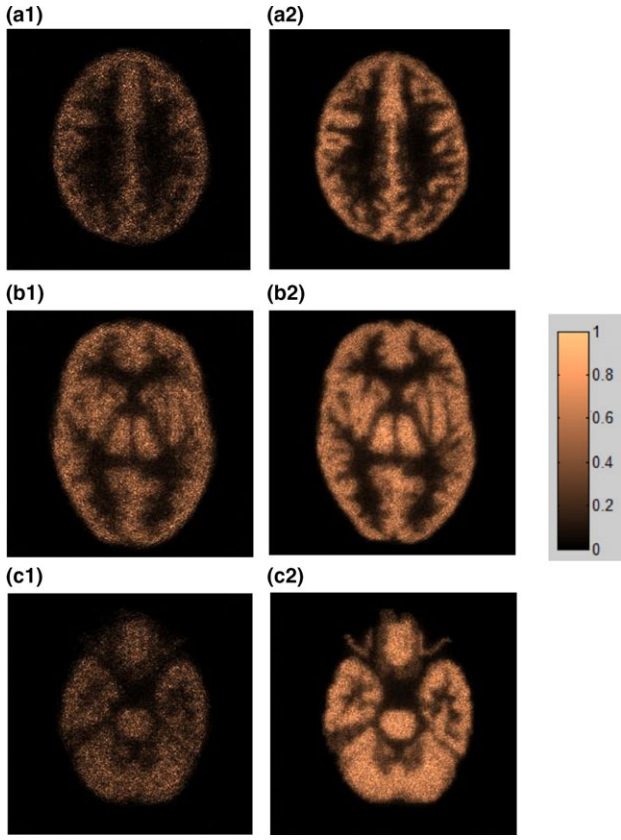

FIG. 9. The reconstructed images of the Hoffman phantom for the HRRT system (top row) and the dodecahedral system (bottom row). (a) Top slice. (b) Center slice. (c) Bottom slice. [Color figure can be viewed at wileyonlinelibrary.com]

4. DISCUSSION

This work simulated a high-sensitivity brain PET system. The system has a great improvement in sensitivity respect to the HRRT system and the helmet system.[13] The peak-NECR of the proposed system is significantly improved compared to

the HRRT system and the helmet-chin system[14] (see Table IV) due to the increased sensitivity. The CRC of our proposed system is slightly better than that of the HRRT system. Furthermore, the dodecahedral system provides images with less noise than the HRRT system and shows higher CNR values. Although a detailed comparison will be conducted in the future, based on our simulation, we notice that the dodecahedral system also outperforms the brain PET with four-layer MPPC DOI detectors in terms of sensitivity,[8] since the latter (2.14%) has lower sensitivity than the HRRT system (2.5%).[6]

For a compact design such as the dodecahedral system, DOI information is critical to the image quality. The HRRT system used 10 mm LSO and 10 mm LYSO for DOI; the helmet-chin system used four layers in the 20 mm crystal; and Gong et al.[13] simulated the helmet system with three layers of crystal, which made the DOI resolution 6.67 mm; the ring PET[8] with four-layer MPPC DOI detectors was designed with crystal lengths 3, 4, 5, and 8 mm for each layer. In our resolution comparison (Figs. 4 and 5), when the DOI resolution is 6.67 mm, the dodecahedral system achieves a slightly better spatial resolution than the HRRT, helmet, and helmet-chin systems. Thus, we chose this three-layer DOI in other simulations. However, the ring PET[8] with four-layer MPPC DOI detectors shows even better resolution thanks to the smaller crystal sectional area (1.2×1.2 mm^2) and the shorter crystal lengths.

In order for a fair comparison, we simulated both HRRT and the dodecahedral system in GATE. However, the simulations of the helmet and helmet-chin geometries are not trivial. We thus only borrowed results from literatures. Meanwhile, for HRRT and the dodecahedral system, we simulated the same phantom and matched the acquisition conditions as in those literatures. For instance, when comparing overall sensitivity, we simulated a big cylinder water phantom to be consistent with the one in *Gong* et al.[13] This is different from what is suggested by NEMA and resulted in lower sensitivity for the HRRT system than that in Sossi et al.[5] When NECR was concerned, the same scenario was simulated as in the helmet-chin PET, which used a hemisphere with a radius of 114 mm instead of line sources. With different phantoms, the value is different while the trend is similar. For instance, the trend of CRC values for HRRT agree with that in Sossi et al.[5]

This work provided detailed simulations for a brain PET system under construction. There are a few issues to be improved both in software design and hardware design. Images in Figs. 5, 7 and 9 were reconstructed with all detected events in the energy window of 250–750 keV, including true and scattered events. For both HRRT and the proposed system, no scatter correction has been done in this work. While scatter correction is necessary given the high fraction of scattering photons. Meanwhile, the scanner is simulated with pixelated crystals of 2 mm, which limits the spatial resolution of the reconstructed images. We plan to use monolithic crystals to further improve the resolution and compare the performance with the four-layer MPPC PET.

5. CONCLUSION

We have performed simulation studies to evaluate the performance of a dodecahedral PET scanner for brain imaging and compared it with three other dedicated brain PET scanners. Our study shows that the proposed system improves the overall sensitivity by a factor of 4.91 compared with the cylindrical brain PET system (e.g., HRRT) and by a factor of 72% compared with the helmet system designed by Gong et al. The proposed system also increases the peak-NECR by 1.61 times compared to the helmet-chin scanner and by 1.25 times compared to the HRRT scanner. Reconstructed phantom images demonstrated high image quality with DOI information. With a DOI resolution being 6.67 mm, the proposed system achieves best spatial resolution of 1.98 mm near the center, better contrast recovery ability, and higher contrast-to-noise ratio than the HRRT system. Using a Hoffman phantom we also demonstrated the potential clinical application of the proposed system.

ACKNOWLEDGMENT

This work was supported by the National Science Foundation of China under Grant No. 51627807.

CONFLICT OF INTEREST

The authors have no conflicts to disclose.

[a)]Author to whom correspondence should be addressed. Electronic mails: qpeng@lbl.gov; jfxu@hust.edu.cn and qiuhuang@sjtu.edu.cn.

REFERENCES

1. Cho ZH, Son YD, Choi EJ, et al. In-vivo human brain molecular imaging with a brain-dedicated PET/MRI system. *Magn Reson Mater Phy.* 2013;26:71–79.
2. Karp JS, Surti S, Freifelder R, et al. Performance of a GSO brain PET camera. Nuclear Science Symposium Conference Record; 2000:17/7-1711, vol. 3.
3. Cho ZH, Hong KS, Hilal SK. Spherical positron emission tomograph (S-PET) I - performance analysis. *Nucl Instrum Methods Phys Res*. 1984;225:422–438.
4. Reske SN, Kotzerke J. FDG-PET for clinical use. *Eur J Nucl Med*. 2001;28:1707–1723.
5. Sossi V, De Jong HWAM, Barker WC, Bloomfield P. The second generation HRRT - a multi-centre scanner performance investigation. Nuclear Science Symposium Conference Record; 2005:2195–2199.
6. De Jong HW, Van Velden FH, Kloet RW, Buijs FL, Boellaard R, Lammertsma AA. Performance evaluation of the ECAT HRRT: an LSO-LYSO double layer high resolution, high sensitivity scanner. *Phys Med Biol*. 2007;52:1505–1526.
7. Omura T, Moriya T, Yamada R, et al. Development of a high-resolution four-layer DOI detector using MPPCs for brain PET. Nuclear Science Symposium and Medical Imaging Conference; 2012:3560–3563.
8. Watanabe M, Saito A, Isobe T, et al. Performance evaluation of a high-resolution brain PET scanner using four-layer MPPC DOI detectors. *Phys Med Biol*. 2017;62:7148.
9. Pajak MZ, Volgyes D, Pimlott SL, et al. NEMA NU4-2008 performance evaluation of Albira: a two-ring small-animal PET system using continuous LYSO crystals. *Open Med J*. 2016;3:12–26.

10. Son YD, Kim HK, Kim ST, Kim NB, Kim YB, Cho ZH. Analysis of biased PET images caused by inaccurate attenuation coefficients. *J Nucl Med*. 2010;51:753–760.
11. Pickut BA, Dierckx RA, Dobbeleir A, et al. Validation of the cerebellum as a reference region for SPECT quantification in patients suffering from dementia of the Alzheimer type. *Psychiatry Res*. 1999;90:103–112.
12. Chatziioannou A, Dahlbom M. Study of the effects of whole body PET spatial sampling schemes on data SNR. Nuclear Science Symposium Conference Record; 2002:1295–1299, vol. 2.
13. Gong K, Majewski S, Kinahan PE, et al. Designing a compact high performance brain PET scanner-simulation study. *Phys Med Biol*. 2016;61:3681.
14. Tashima H, Yoshida E, Nishikido F, et al. Development of the helmet-chin PET prototype. Nuclear Science Symposium and Medical Imaging Conference; 2016:1–3.
15. Tashima H, Yamaya T. Proposed helmet pet geometries with add-on detectors for high sensitivity brain imaging. *Phys Med Biol*. 2016;61:7205.
16. Ahmed AM, Tashima H, Yoshida E, Yamaya T. Investigation of the optimal detector arrangement for the helmet-chin PET – a simulation study. *Nucl Instrum Methods Phys Res*. 2017;858:96–100.
17. Ahmed AM, Tashima H, Yoshida E, Nishikido F, Yamaya T. Simulation study comparing the helmet-chin PET with a cylindrical PET of the same number of detectors. *Phys Med Biol*. 2017;62:4541.
18. Moghaddam NM, Karimian A, Mostajaboddavati SM, Vondervoort E, Sossi V. Preliminary design and simulation of a spherical brain PET system (SBPET) with liquid xenon as scintillator. *Nukleonika*. 2009;54:33–38.
19. Bao Q, Cho S, Li Q, Newport D. Monte Carlo based estimation of detector response in a large solid angle Preclinical PET imaging system. IEEE Nuclear Science Symposium Conference Record; 2008:5010–5013.
20. Shi H, Du D, Xu J, Su Z, Peng Q. Design study of dedicated brain PET with polyhedron geometry. *Technol Health Care*. 2015;23:S615.
21. Jan S, Santin G, Strul D, et al. Gate: a simulation toolkit for PET and SPECT. *Phys Med Biol*. 2004;49:4543.
22. Rademakers F, Brun R. ROOT: an object-oriented data analysis framework. *Nucl Instrum Methods Phys Res*. 1998;389:81–86.
23. Kao CM, Dong Y, Xie Q. Evaluation of 3D image reconstruction methods for a dual-head small-animal PET scanner. Nuclear Science Symposium Conference Record; 2008:3046–3050.
24. Kao CM, Pan X, Chen CT. Accurate image reconstruction using DOI information and its implications for the development of compact PET systems. *IEEE Trans Nucl Sci*. 2002;47:1551–1560.
25. Jaszczak RJ. Nuclear imaging phantom. US 4499375 A; 1985.
26. Hoffman EJ, Cutler PD, Digby WM, Mazziotta JC. 3-D phantom to simulate cerebral blood flow and metabolic images for PET. *IEEE Trans Nucl Sci*. 1990;37:616–620.
27. Huesman RH, Klein GJ, Moses WW, Qi J. List-mode maximum-likelihood reconstruction applied to positron emission mammography (PEM) with irregular sampling. *IEEE Trans Med Imaging*. 2000;19:532–537.
28. Jan S, Comtat C, Strul D, Stantin G, Trebossen R. Monte Carlo simulation for the ECAT EXACT HR+ system using GATE. *Trans Nucl Sci*. 2005;52:627–633.
29. Rausch I, Cal-González J, Dapra D, et al. Performance evaluation of the Biograph mCT Flow PET/CT system according to the NEMA NU2-2012 standard. *Ejnmmi Phys*. 2015;2:1–17.
30. Thielemans K, Tsoumpas C, Mustafovic S, et al. STIR: software for tomographic image reconstruction release 2. Nuclear Science Symposium Conference Record. IEEE, 2174-2176; 2012.
31. Strother SC, Casey ME, Hoffman EJ. Measuring PET scanner sensitivity: relating countrates to image signal-to-noise ratios using noise equivalents counts. *IEEE Trans Nucl Sci*. 1990;37:783–788.
32. Hart HJ, Bottomley PA, Edelstein WA, et al. Nuclear magnetic resonance imaging: contrast-to-noise ratio as a function of strength of magnetic field. *Magn Reson Imaging*. 1983;2:1195.